Design Considerations for Miniaturized Control Moment Gyroscopes for Rapid Retargeting and Precision Pointing of Small Satellites

Kunal Patankar, Norman Fitz-Coy
University of Florida
1064, Center Drive, #185; 352 846 3020
Kunal.patankar@ufl.edu

Carlos M. Roithmayr
NASA Langley Research Center
Mail Stop 451; 757 864 6778
carlos.m.roithmayr@nasa.gov

ABSTRACT

This paper presents the design as well as characterization of a practical control moment gyroscope (CMG) based attitude control system (ACS) for small satellites in the 15-20 kg mass range performing rapid retargeting and precision pointing maneuvers. The paper focuses on the approach taken in the design of miniaturized CMGs while considering the constraints imposed by the use of commercial off-the-shelf (COTS) components as well as the size of the satellite. It is shown that a hybrid mode is more suitable for COTS based moment exchange actuators; a mode that uses the torque amplification of CMGs for rapid retargeting and direct torque capabilities of the flywheel motors for precision pointing. A simulation is provided to demonstrate on-orbit slew and pointing performance.

Miniaturization and advances in electronics have generated a significant interest in small satellites. Many applications such as high-resolution imaging, and Earth and space monitoring are being envisioned for such systems[1,2]. These applications may impose the need for rapid retargeting, as well as precision pointing, on these small satellites.

Typically, the mission of the satellite will demand certain higher level performance specifications; e.g., rapid retargeting of the satellite will dictate the angular momentum and torque output of the actuator, whereas precision pointing will dictate the torque accuracy. As the scope of this design process is to develop a control moment gyroscope (CMG) based attitude control system (ACS) system suitable for a broad range of operations over multiple satellite platforms, exact higher level requirements are not directly available. Thus, an attempt has been made to put realistic limits on the pointing requirements of the satellite based on its size and mass as well the payload/mission objectives.

This paper discusses the design of a practical ACS for small satellites in 15-20 kg mass range using commercial-off-the-shelf (COTS) components. The paper is organized as follows. First, the details of the satellite for which this ACS is being designed are provided. Then slew and pointing accuracy requirements for this satellite are discussed. The size of the satellite also imposes constraints on the mass, volume, and available power. These provide baseline performance parameters for the ACS such as stored angular momentum and torque. Commercially available motors are then analyzed for their suitability for the CMG flywheel and gimbal. The motors are then analyzed for the torque accuracy and a control strategy that takes advantage of gyroscopic as well as direct torques is discussed.

Details of the satellite

The discussions that follow are generic to small satellites but for discussion purposes we consider the representative satellite shown in Figure 1. This 12U-class satellite has dimensions 250 mm x 250 mm x 340 mm, mass 20 kg, and centroidal inertias of $I_{xx} = I_{yy} = 0.3\ \text{kg} \cdot \text{m}^2$ and $I_{zz} = 0.21\ \text{kg.m}^2$. Body mounted solar cells were assumed in the inertia calculations. A quick

survey of commercially available satellite hardware has shown that, for this class of the satellite, it is possible to have agile imaging satellites; i.e., within the size, weight, and power (SWaP) constraints of this class of satellites it is possible to have an optical bench, attitude determination and control system, sufficient power generation and storage capacity, as well as high data rate communication.

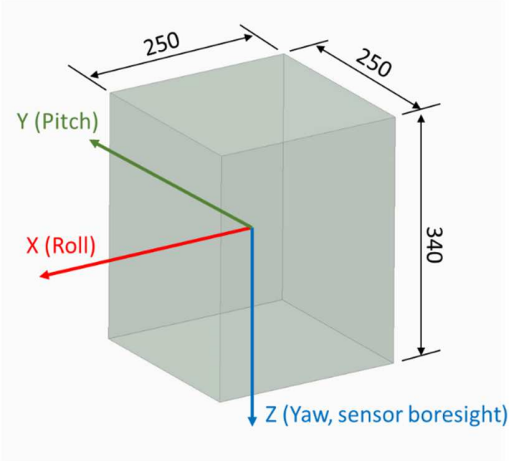

Figure 1. Representative small satellite

Typically, imaging requires attitude stability on the order of a few arc seconds whereas the communication link can tolerate attitude instability of few arc minutes. Different imaging modes may demand slew rates from 0.1 deg/s to 10 deg/s. Thus, an imaging payload is assumed for the estimation of slew rate and pointing precision. Satellite altitude is assumed to be between 350 and 700 km. It is worth noting that a 350-km altitude represents the lowest altitude where an orbital life of a few years can be achieved with periodic altitude maintenance; however, altitude maintenance is not the focus of this paper.

Satellite slew requirements

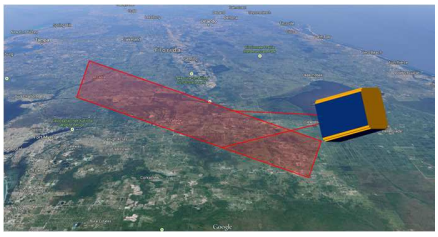

(a) Strip imaging

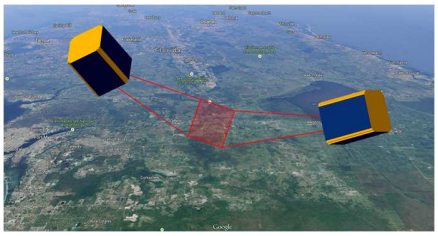

(b) Stereoscopic imaging

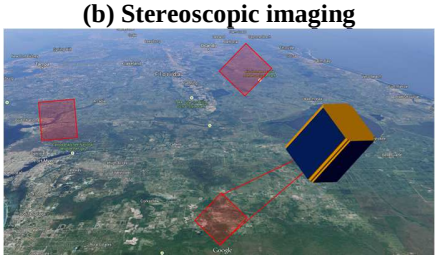

(c) Spot imaging

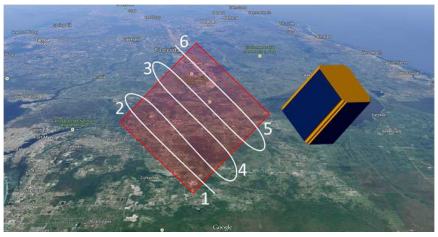

(d) area imaging

Figure 2 Typical satellite imaging modes

Slew requirements directly dictate the torque output of the actuator. Satellite slew requirements are dependent on the imaging mode. Figure 2 shows four imaging modes: strip imaging, stereoscopic imaging, spot imaging, and area imaging. These four modes demand different slew rates. Strip imaging involves scanning the Earth's surface as the satellite moves along its path; this can be achieved by maintaining a fixed orientation with respect to nadir for the imaging duration, and thus it requires a slew that matches the orbital angular velocity. For the altitudes under consideration it is less than 0.1 deg/s. Stereoscopic imaging requires pointing at the same spot from two positions in the orbit and may need slew rates of 0.5 to 1 deg/s. The other two modes may demand much higher slew rates. In the spot mode, the actual slew rate is dependent on the number of spots and angular separation between them. Area imaging involves rapid slew along roll and pitch axis to artificially widen the swath. The satellite slews along the path 1-6 and creates a composite image from multiple images captured during the process. A slew rate of 15 deg/s is assumed to be sufficient for these two modes.

Reference 3 discusses implementation of these modes on the NigeriaSat-2 satellite.

Satellite pointing requirements

Satellite pointing requirements dictate the torque accuracy of the ACS system; this CMG system design parameter is critical and difficult to quantify.

Let's assume that satellite altitude is alt and the spatial resolution of the imaging system is w. Using a small angle approximation, the angular distance, ψ, that corresponds to the linear distance of w when viewed from distance alt is given by $\psi \cong \frac{w}{alt}$.

The spatial resolution is assumed to be in the range of 25 to 75 m. The angular resolution is directly proportional to the spatial resolution and inversely proportional to the satellite altitude and it is between 7 and 45 arc seconds for the selected parameters.

Power and size/mass limitations

The size of the satellite limits the available power as well as volume and mass that can be allotted to the CMGs and this must be taken into account while selecting the hardware.

If we assume that side panels of the satellite have 80% coverage with high efficiency solar cells (28% efficiency assumed) and only one side faces the sun, the maximum power that can be generated is approximately 26 watts. Assuming a 30% eclipse period per orbit, the average on-orbit power is 18 watts. The eclipse period is a function of the orbital parameters and varies greatly. For example, the dawn-dusk sun synchronous orbit has no eclipse period whereas a 350-km equatorial orbit has a 40% eclipse period. If deployable panels are used, the power can be higher but the flexibility introduced by the panels may limit the maximum slew rate. Thus, body mounted panels are considered for this design.

The power that can be allotted to the ACS is assumed to be 20% of average on-orbit power and it is expected that the mass and size of the system is within 15% of the available mass and size. The other power consuming satellite subsystems (e.g., communications and imager payload) are usually duty cycled, thus, allotting a higher percentage of available power to the ACS can be justified. It must be noted that these assumptions are only to provide approximate guidelines for the hardware selection.

Design parameters of the ACS

CMG configuration

A pyramidal CMG configuration with a pyramid angle, θ, of 54.74 degrees is considered. This configuration has a nearly spherical angular momentum envelope. The actual normalized angular momentum for this arrangement is shown in Figure 3 and varies between approximately $2.4h$ and $3.2h$, where h is the angular momentum of each flywheel.

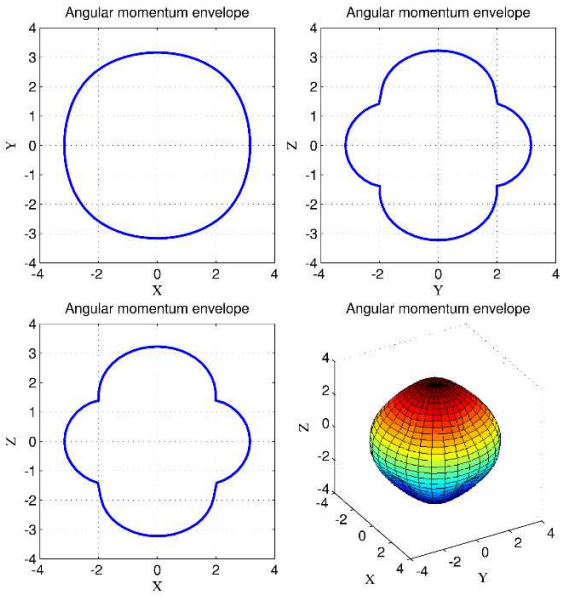

Figure 3. Normalized angular momentum

Angular momentum of flywheels

Assuming the maximum required slew rate of the satellite about its pitch (or roll) axis is 15 deg/s (0.26 rad/s), the magnitude of the total angular momentum of the satellite is

$$H = I_{yy}\omega = I_{xx}\omega = 0.078\ \text{kg} \cdot \text{m}^2 \cdot \text{s}^{-1}$$

Now, this momentum must be transferred from the ACS. Considering the lower limit of $2.4h$ for the momentum transfer, and adding a 25% safety margin, then the angular momentum of each CMG is $h = 0.04\ \text{kg} \cdot \text{m}^2\text{s}^{-1}$

Hardware selection

Proper selection of gimbal and flywheel motors is essential for the correct ACS operation. In this effort, three types of motors are considered: brushed DC motors, brushless DC motors, and stepper motors.

Brushed DC motors are easiest to control but as the commutation is through brushes, the operational life of the motor is limited. The fine dust produced by the brushes is also a concern in the microgravity environment. Brushless DC motors have electronic commutation but require complex control electronics for controlling. For slow speeds and/or low torque ripples, multiple poles are required; e.g., the brushless DC motor of Hubble telescope fine pointing mechanism has 24 poles and has just 0.2% torque ripples[4]. However, such motors are custom designed and are typically not available as COTS. Most of the COTS brushless DC motors have 2 or 4 poles. Stepper motors are suitable when movement in discrete steps is needed.

The unique requirements of the flywheel and gimbal motors are outlined below.

Flywheel motor

Flywheel motors must keep the flywheels running continuously over the operational life of the satellite. The speeds under consideration are up to 15,000 RPM. As continuous operation at high speeds is desired, a brushless DC (BLDC) motor is the only suitable option. A BLDC flywheel motor is selected based on the following criteria

- **Torque:** Once the flywheels are spun to the desired speed, the torque is needed only to counter bearing friction.
- **Efficiency:** High-efficiency motors are desirable since (i) the available power is limited and (ii) the losses through heat generation are minimized, thus enabling more design flexibility (from a thermal perspective).
- **Environmental considerations:** Ability to operate in the hard vacuum and use of low outgassing materials in the construction of the motor.
- **Operating voltage:** An operating voltage of 12V or less would allow it to be compatible with most of the small satellite power systems.

Gimbal motor

The gimbal motor is required to reorient the flywheel axis at the desired rate and to the desired orientation. The gimbal motor is selected based on following criteria

- **Speed range and gear head compatibility**: Typical gimbal rates are in the range of 0-60 deg/s. Since the magnitude of the output torque of the CMG is the product of flywheel angular momentum and gimbal speed, very low gimbal speeds are desirable as they dictate the minimum gyroscopic torque output of the CMG. It is impractical to drive the gimbals directly using brushed DC or BLDC as COTS motors are typically not designed for such low speed and they must be paired with a gear train. A gear train with high gear ratio, 200:1 or more must be used so that the minimum speeds up to 0.25 deg/s can be achieved. The gearhead must be selected such that it has zero or minimum backlash.
- **Speed control:** The torque accuracy of the CMG depends on the speed control as any gimbal speed error directly translates to the torque error. Speed control depends not only on the motor but also on the encoder resolution and backlash in the gear train, if any. Stepper motors also face another problem when it comes to the speed control since they move in discrete steps, which results in torque ripples in the CMG torque output.
- **Efficiency:** Efficiency of the gimbal motors is not as critical as flywheel motors since motor use is intermittent.
- **Operating voltage:** As is the case for the flywheel motor, an operating voltage of 12V or less is desirable.

Based on these criteria, it was decided to test all three types of motors for their actual performance before incorporating any one into a design.

Torque and pointing accuracy

Since gimbal speeds as well as flywheel speeds are maintained using feedback control, it is essential to investigate the sensitivity of the control torques to these speed errors. This investigation was conducted through simulations. Based on the previously calculated value of

$h = 0.04$ Nms, we assume a nominal flywheel speed of 12,000 RPM (1257 rad/s) and a corresponding flywheel inertia of 32×10^{-6} kgm^2.

Effect of flywheel speed variation

Variations in the flywheel speed dictate the angular momentum stability of the CMG. A preliminary review of existing COTS hardware indicates that the speed can be maintained within 0.1% of the nominal speed. Even at this precise speed control, the contribution of the flywheel speed variation to the torque error is larger than the other error sources. The torque error due to flywheel speed variation is shown in Figure 4. The flywheel speed error is assumed to follow a normal distribution with 2-sigma limits of 12 RPM. However, this torque error is at the flywheel speed (200 Hz) and can be filtered using an appropriate damping mechanism.

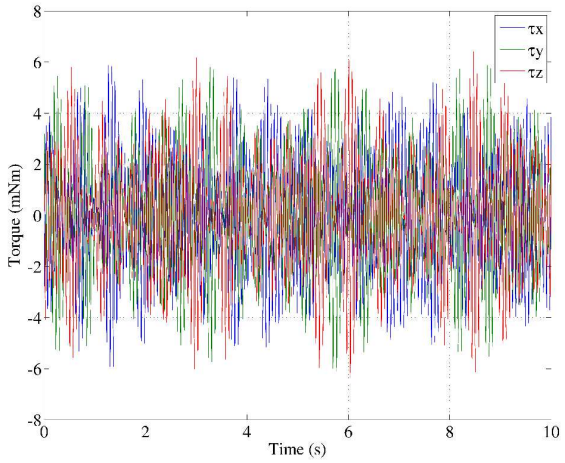

Figure 4. Torque error due to flywheel speed variation

Effect of gimbal speed and position inaccuracy

The effects of gimbal speed variations and position inaccuracy on torque are shown in Figure 5. Although the actual orientation of the gimbals largely dictate the exact torque error, Figure 5 provides an order of magnitude estimate of this error. A BLDC with zero backlash gear head is considered for this analysis and for subsequent simulations. The review of the COTS motors indicated that the gimbal speed is controllable within 0.05 deg/s of the desired speed and the error in the gimbal position knowledge is 0.01 degrees.

The curves shown in Figure 5 represent the difference between computed torque output of the CMG cluster and commanded torque when gimbal speed errors were assumed to follow normal distribution with 2-sigma limits of 0.05 deg/s. The gimbal position was obtained by integrating the gimbal speed. The maximum torque of the CMG cluster is approximately 120 mNm, so in this case, the torque error due to gimbal speed and position error is approximately 0.5% of the maximum torque.

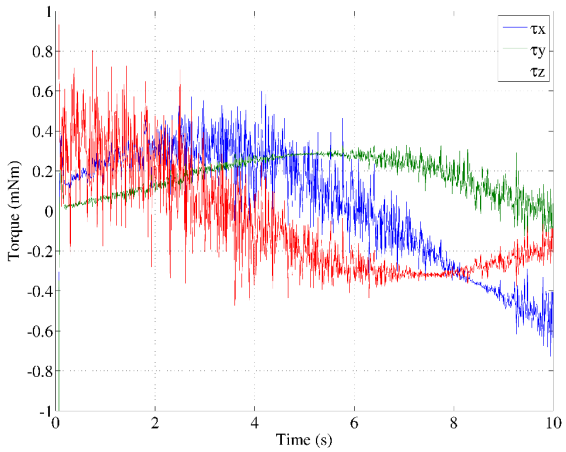

Figure 5. Torque error due to gimbal speed and position inaccuracy

Another parameter that limits the effectiveness of the CMGs is the dead zone. Figure 6 shows the torque output of a single CMG with a sinusoidal gimbal speed profile. Gimbal speeds slower than 0.25 deg/s are difficult to achieve with COTS components and it restricts the lower limit of the torque. For the scenario considered, torques smaller than 0.1 mNm cannot be achieved.

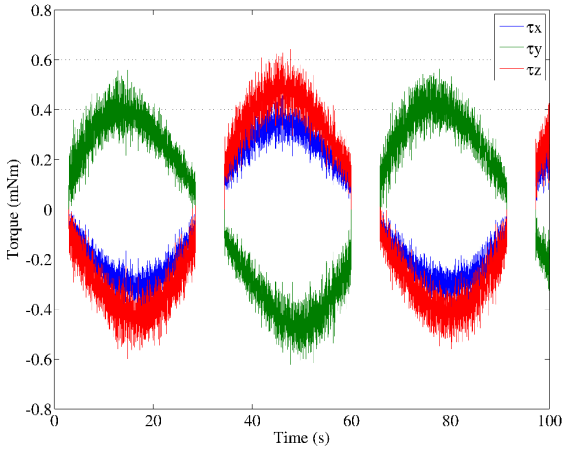

Figure 6. Effect of dead zone on the torque

Effect of flywheel acceleration error

Assuming flywheel acceleration error can be controlled within 10% of the commanded acceleration, for a commanded acceleration of 2 rad/s^2 the torque error is on the order of 0.01 mNm. This is significantly less than the torque error due to gimbal speed error. It is shown in the Figure 7.

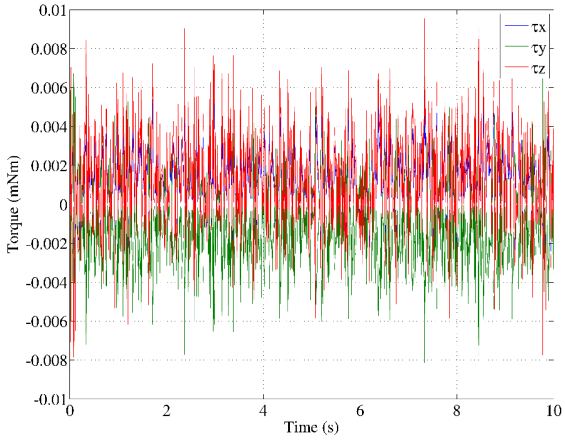

Figure 7. Torque error due to flywheel acceleration error

The discussion above highlights the fact that the gyroscopic mechanism that generates larger torque in CMGs also results in larger torque errors and dead zones. This discussion also highlights that errors associated with RW flywheel accelerations are not as severe as those of the CMGs. Thus, it appears that a hybrid system should be utilized wherein gyroscopic torque (CMGs) is utilized when performing large angle reorientations and flywheel acceleration (RW) is used when precise pointing is required. Such a hybrid system is described below and in references 5-6. When the system is being used in the CMG mode, the flywheels operate at a constant speed and the required torque is generated by gyroscopic effect associated with rotation of the gimbals. When the system is being used in the RW mode, the flywheels are accelerated to generate required torque and gimbals are held at a fixed position.

Hybrid mode

The torque output of a hybrid momentum exchange actuation system is the sum of gyroscopic torque (CMG) and direct torque (RW); i.e.

$$^{B}\boldsymbol{\tau} = {}^{B}\boldsymbol{\tau_G} + {}^{B}\boldsymbol{\tau_D}$$

where $^{B}\boldsymbol{\tau_G} = I_w \boldsymbol{A}\hat{\boldsymbol{\Omega}}\dot{\boldsymbol{\delta}}$ is the gyroscopic torque and $^{B}\boldsymbol{\tau_D} = I_w \boldsymbol{B}\dot{\boldsymbol{\Omega}}$ is the direct torque. I_w is the centroidal moment of inertia of the flywheel about its spin axis, $\hat{\boldsymbol{\Omega}} = diag(\Omega_1, \Omega_2, \Omega_3, \Omega_4)$, $\dot{\boldsymbol{\Omega}} = [\dot{\Omega}_1, \dot{\Omega}_2, \dot{\Omega}_3, \dot{\Omega}_4]^T, \dot{\boldsymbol{\delta}} = [\dot{\delta}_1, \dot{\delta}_2, \dot{\delta}_3, \dot{\delta}_4]^T$ where Ω_i is the angular speed of the ith flywheel and $\dot{\delta}_i$ is its gimbal speed.

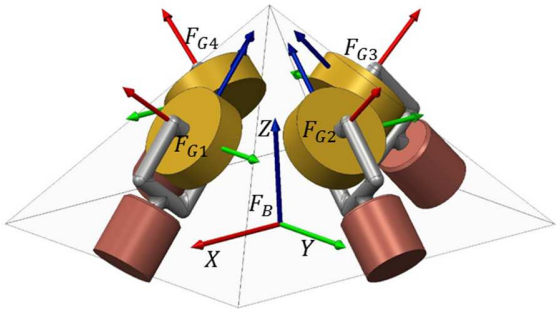

Figure 8. Pyramidal CMG configuration

Matrices ***A*** and ***B*** map, respectively, the gyroscopic and direct torques of the actuators from the CMG frame (F_{Gi} , $i = 1$ to 4) to the satellite body frame (F_B). For the pyramidal configuration shown in **Figure 8**, the gimbal spacing angles are $\phi = [0, 90, 180, 270]^T$ degrees, the pyramid angle is θ and the gimbal angles are $\delta = [\delta_1\ \delta_2\ \delta_3\ \delta_4]^T$; for this configuration, matrices ***A*** and ***B*** are:

$$\boldsymbol{A} = \begin{bmatrix} -\cos\theta\sin\delta_1 & -\cos\delta_2 & \cos\theta\sin\delta_3 & \cos\delta_4 \\ \cos\delta_1 & -\cos\theta\sin\delta_2 & -\cos\delta_3 & \cos\theta\sin\delta_4 \\ \sin\theta\sin\delta_1 & \sin\theta\sin\delta_2 & \sin\theta\sin\delta_3 & \sin\theta\sin\delta_4 \end{bmatrix}$$

$$\boldsymbol{B} = \begin{bmatrix} \cos\theta\cos\delta_1 & -\sin\delta_2 & -\cos\theta\cos\delta_3 & \sin\delta_4 \\ \sin\delta_1 & \cos\theta\cos\delta_2 & -\sin\delta_3 & -\cos\theta\cos\delta_4 \\ -\sin\theta\cos\delta_1 & -\sin\theta\cos\delta_2 & -\sin\theta\cos\delta_3 & -\sin\theta\cos\delta_4 \end{bmatrix}$$

Reference 5 provides a detailed mathematical model of the hybrid CMG and development of these matrices.

Singularity analysis

It is well known that CMGs suffer from internal singularities wherein a torque cannot be produced in a specified direction. Mathematically, this occurs when matrix ***A*** becomes rank deficient. For example, consider a set of gimbal angles $[0,0,0,0]^T$. The torque that can be produced with this gimbal angle configuration is limited to xy-plane of the satellite since

$$^{B}\boldsymbol{\tau_G} = I_w \begin{bmatrix} 0 & -1 & 0 & 1 \\ 1 & 0 & -1 & 0 \\ 0 & 0 & 0 & 0 \end{bmatrix} \begin{bmatrix} \dot{\Omega_1}\delta_1 \\ \Omega_2\dot{\delta}_2 \\ \Omega_3\dot{\delta}_3 \\ \Omega_4\dot{\delta}_4 \end{bmatrix}$$

$$^{B}\boldsymbol{\tau_G} = I_w \begin{bmatrix} \Omega_4\dot{\delta}_4 - \Omega_2\dot{\delta}_2 \\ \Omega_1\dot{\delta}_1 - \Omega_3\dot{\delta}_3 \\ 0 \end{bmatrix}$$

and in this case it can be shown that $\boldsymbol{A}$ has rank 2

This CMG singularity has been extensively studied and there are various control laws that either avoid these singular configurations or escape these singularities by applying a torque error [7-15].

However, the hybrid approach introduces a new kind of singularity, one that is associated with the RWs. Typically, when only RW based attitude control is used the orientations of the wheels are predetermined and fixed such that torque along any desired direction can be commanded. In the hybrid mode, however, the control strategy is to switch at the end of the rapid slew maneuver from CMG mode to a RW mode to provide precision tracking performance. Thus, the orientation of the gimbals at the end of a rapid slew must be such that the RWs are able to produce the desired torque. For example, consider the gimbal angle configuration $[90,90,90,90]^T$. The torque that can be produced by flywheel motors at this gimbal angle configuration is limited to the xy-plane of the satellite since

$$^{B}\boldsymbol{\tau_D} = I_w \begin{bmatrix} 0 & -1 & 0 & 1 \\ 1 & 0 & -1 & 0 \\ 0 & 0 & 0 & 0 \end{bmatrix} \begin{bmatrix} \dot{\Omega}_1 \\ \dot{\Omega}_2 \\ \dot{\Omega}_3 \\ \dot{\Omega}_4 \end{bmatrix}$$

$$^{B}\boldsymbol{\tau_D} = I_w \begin{bmatrix} \dot{\Omega}_4 - \dot{\Omega}_2 \\ \dot{\Omega}_1 - \dot{\Omega}_3 \\ 0 \end{bmatrix}$$

and in this case it can be shown that **B** has rank 2

In the RW mode, the desired torque is mapped onto the flywheel acceleration as

$$\dot{\boldsymbol{\Omega}} = \frac{1}{I_w}\boldsymbol{B}^T(\boldsymbol{B}\boldsymbol{B}^T)^{-1}\,{}^{B}\boldsymbol{\tau_D}$$

The torque cannot be mapped onto the flywheel acceleration if $\boldsymbol{B}\boldsymbol{B}^T$ is singular, thus this quantity can be used as a singularity parameter. Let S be the singularity parameter defined as,

$$S = det(\boldsymbol{B}\boldsymbol{B}^T)$$

A steering law that uses this singularity parameter to drive gimbals away from the RW singularity is discussed in the following section.

Steering law

The steering algorithm under consideration is a combination of a GSR (Generalized Singularity Robust) steering law [12] and null motion. The torque is mapped onto the gimbal rates or flywheel acceleration as follows.

$$\dot{\boldsymbol{\delta}} = \alpha(I_w\widehat{\boldsymbol{\Omega}})^{-1}[\boldsymbol{A}^T(\boldsymbol{A}\boldsymbol{A}^T + \lambda\boldsymbol{E})^{-1}\boldsymbol{\tau} + \beta\mathbf{d}]$$

$$\dot{\boldsymbol{\Omega}} = (1-\alpha)I_w^{-1}\boldsymbol{B}^T(\boldsymbol{B}\boldsymbol{B}^T)^{-1}\boldsymbol{\tau}$$

where $\boldsymbol{d}$ is the null vector, and α is the mode switch parameter, which is externally selected. It is between 0 and 1. It can be binary (i.e. either 1 or 0), which will cause an instantaneous mode switch, or it can gradually change from 1 to 0 for a more gradual mode change. The simulations presented in this paper use gradual change. λ and β are CMG and RW singularity parameters, respectively, and are defined as follows

$$\lambda = \lambda_0 \exp(-\mu_1 det(\boldsymbol{A}\boldsymbol{A}^T))$$

$$\beta = \beta_0 \exp(-\mu_2 det(\boldsymbol{B}\boldsymbol{B}^T))$$

The CMG singularity parameter introduces torque error to steer the gimbals away from a CMG singularity and the RW singularity parameter adds null motion to steer the gimbals away from a RW singularity. Tuning parameters λ_0 and β_0 dictate the maximum value of each singularity parameter, and μ_1 and μ_2 dictate how rapidly the singularity parameters fall off as the system moves away from a singularity. The choice of the parameters influences the behavior of the control law and are typically tuned by the designer. Table 1 lists the values used for the simulation. Matrix E adds a time varying component to the torque error, which allows escape from the gimbal lock condition if it is encountered.

Simulation

Multiple Matlab simulations were performed to demonstrate the behavior of the hybrid steering logic. Table 1 lists the simulation parameters.

A block diagram of the simulation is shown in Figure 9. Quaternions are used as attitude parameters. $[\boldsymbol{\epsilon}\ \eta]^T$ represents satellite attitude and $[\boldsymbol{\epsilon}_d\ \eta_d]^T$ represents desired attitude. The initial attitude of the satellite is denoted by $[\boldsymbol{\epsilon}_i\ \eta_i]^T$ Perfect attitude knowledge is assumed for the feedback. Quaternion feedback regulator[16] which allows rest-to-rest least angle reorientation between two attitudes is used as a controller with K_p as proportional gain and K_d as derivative gain.

Four simulations are discussed in this section. All simulations consist of a rest-to-rest rapid retargeting and precision pointing (R2P2) maneuver: the satellite is commanded to reorient by 30 degrees. The initial direction of the sensor boresight vector is $[1,0,0]^T$ and final direction is $[\cos(-30),\sin(-30),0]^T$.

The first two simulations are aimed at understanding the hybrid steering law behavior and only the CMG mode is simulated. This is achieved by setting $\alpha = 1$ for the entire duration of the simulation. The objective is to analyze how the RW singularity parameters evolve and how singularity is handled by the hybrid steering law. Also, for these simulations, ideal actuators without torque errors are assumed. That is, there are no flywheel acceleration or gimbal speed/position errors.

The third and fourth simulations incorporate hardware limitations and they focus on the pointing error.

Table 1: Simulation parameters

J	$\begin{bmatrix} 0.3 & 0 & 0 \\ 0 & 0.3 & 0 \\ 0 & 0 & 0.3 \end{bmatrix}$	kgm^2
θ	54	degrees
ϕ	$[0,90,180,270]^T$	degrees
$[\boldsymbol{\epsilon}_i\ \eta_i]^T$	$[\sin(45),0,0,\cos(45)]^T$	
$[\boldsymbol{\epsilon}_d\ \eta_d]^T$	$[\sin(45)\cos(-30),$ $\sin(45)\sin(-30),0,\cos(45)]^T$	
I_w	32 x 10^{-6}	kg-m^2
Ω_0	12000	RPM
K_p	0.4	
K_d	0.4	
λ_0	0.001	
β_0	0.1	
μ_1	-20	
μ_2	-5	
E	$\begin{bmatrix} 1 & e_1 & e_2 \\ e_1 & 1 & e_3 \\ e_2 & e_3 & 1 \end{bmatrix}$	$e_1 = 0.001\sin(t+0.25)$ $e_2 = 0.001\sin(t+0.13)$ $e_3 = 0.001\sin(t+0.05)$

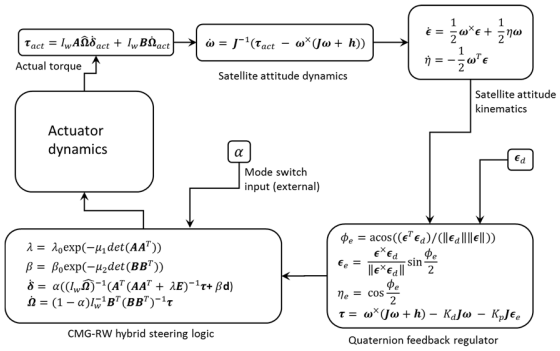

Figure 9. Matlab simulation showing hybrid control logic

Simulation: Case 1

The starting gimbal positions (δ_0) are [80, 80, 80, 80] degrees for this simulation, which is close to a RW singular configuration ([90, 90, 90, 90] degrees). The maneuver causes the gimbals to pass through the RW singularity. The results of a GSR steering law are shown in Figure 10 and results of the hybrid steering law are shown in Figure 11. With the hybrid steering law, the gimbal profile is different than the GSR steering law and the RW singularity parameter at the end of maneuver is larger (0.8 as opposed to 0.25). A larger value of RW singularity parameter implies better control authority.

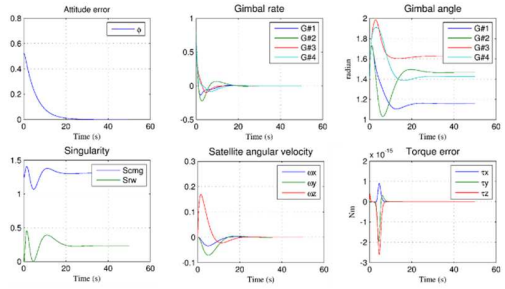

Figure 10 . GSR steering law results for δ_0 = [80, 80, 80, 80] degrees

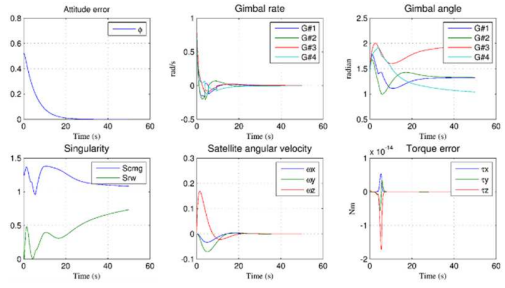

Figure 11. Hybrid steering law results for δ_0 = [80, 80, 80, 80] degrees

Simulation: Case 2

The starting gimbal positions (δ_0) for this simulation are [45, 45, 45, 45] degrees, which is away from an RW singular configuration ([90, 90, 90, 90] degrees). The maneuver does not cause gimbals to go near the singular configuration. The results of the GSR steering law are shown in Figure 12 and results of the hybrid steering law are shown in Figure 13. By comparing the hybrid logic and GSR logic results, it is evident that the hybrid logic adds an insignificant amount of null motion. This is the desired behavior as it minimizes unnecessary gimbal excursions.

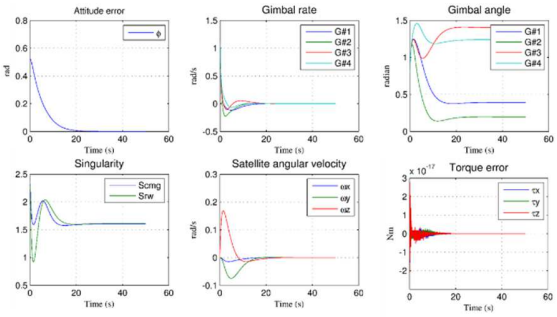

Figure 12. GSR steering law results for δ_0 = [45, 45, 45, 45] degrees

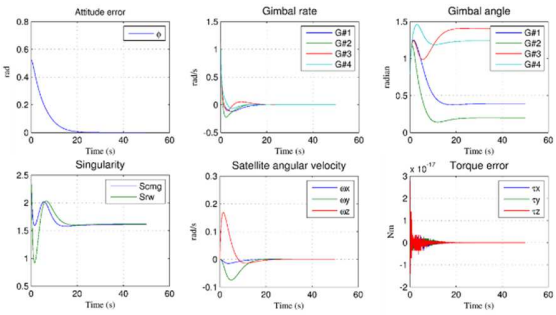

Figure 13. Hybrid steering law results for δ_0 = [45, 45, 45, 45] degrees

These and other simulations have shown that the hybrid steering logic is able to reorient the gimbals such that at the end of reorientation operation, the gimbals are away from the RW singularity.

Simulation: Case 3

The third simulation incorporates flywheel acceleration error and gimbal speed/position errors. The simulation uses GSR steering logic and there is no RW mode. This simulation provides a reference against which the hybrid steering law is later compared. Figure 14 shows the vector part of the error quaternion for the entire duration of the maneuver. Figure 15 shows a magnified view of the steady state error. Due to the CMG torque errors, the quaternion error does not converge to zero and shows a limit-cycle-like behavior. Figure 16 shows the projection of the actual sensor boresight vector on a plane perpendicular to the desired boresight vector. The origin of the plot is the desired pointing direction and the pointing error is in the range of 0.1 degrees (360 arc seconds) in the steady state region.

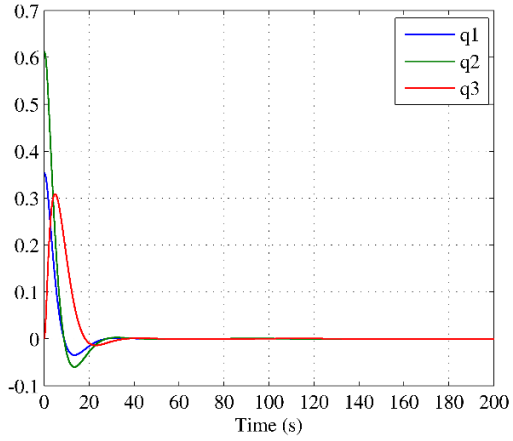

Figure 14: Quaternion error in CMG only mode

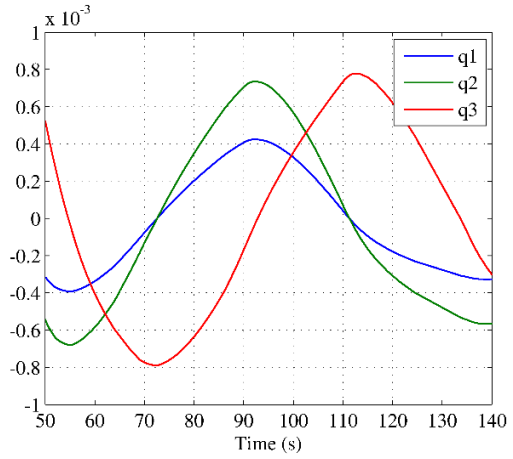

Figure 15: Quaternion error in CMG only mode - steady state region

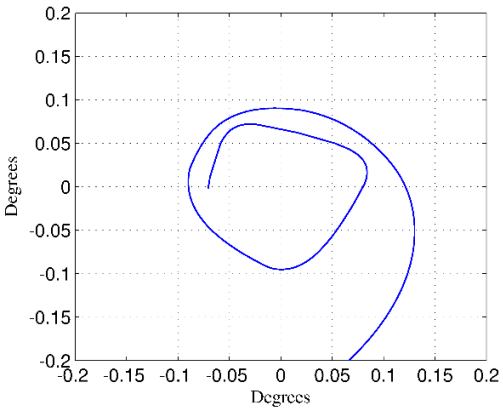

Figure 16: Sensor boresight vector projection in CMG only mode

Simulation: Case 4

The fourth simulation also incorporates flywheel acceleration error and gimbal speed/position errors. It uses the hybrid steering law for the CMG steering. A gradual transition from CMG to RW mode occurs between 100 and 110 seconds.

Figure 17 shows the attitude error in the steady state region and Figure 18 shows a projection of the satellite attitude similar to Figure 16. As soon as the RW mode is actuated, the errors converge to zero.

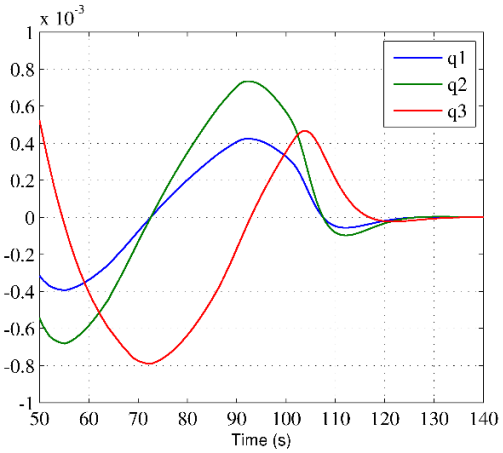

Figure 17: Quaternion error in hybrid mode - steady state region

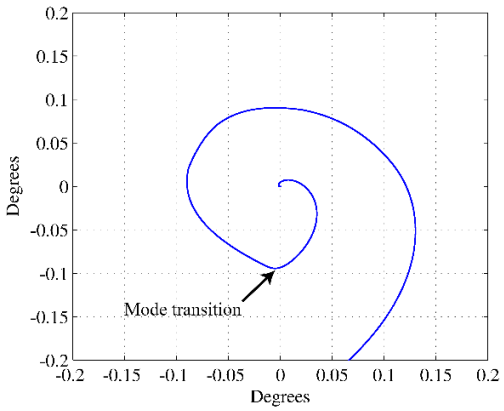

Figure 18: Sensor boresight vector projection in hybrid mode

Figure 19 shows actuator torque error and it is clear that the actuator torque error is larger in the CMG mode than the RW mode. The spikes visible in the CMG mode torque are due to the discontinuous nature of the gimbal motion (dead zone) at slow speeds. Figure 20 shows the flywheel speeds during the transition period. As the torque required during precision pointing is very small, the flywheel speed variations are limited to a few RPMs and it is within the limits of selected motors. High torque motors, which are commonly needed for reaction wheels, are not required.

This simulation shows that in the presence of hardware limitations imposed by COTS components, the pointing performance achieved with the CMG-RW hybrid steering logic is better than that achieved with a CMG-only steering logic.

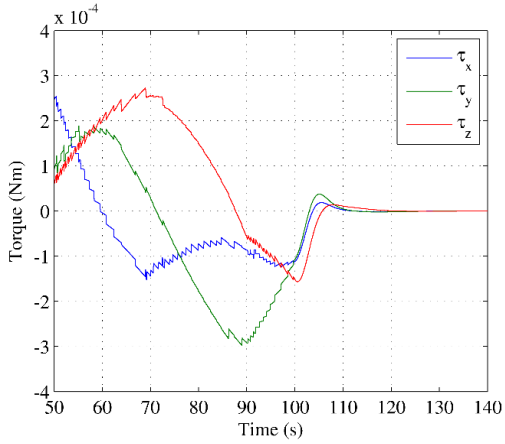

Figure 19: CMG torque in hybrid mode - steady state region

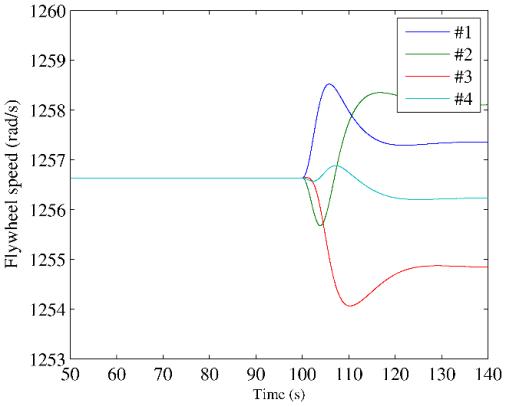

Figure 20: Flywheel speed in hybrid mode - steady state region

Conclusion

An ACS capable of rapid retargeting as well as precision pointing, built from COTS components, will greatly enhance the capability of small satellites. An ACS suitable for satellites in the 15-20 kg mass range is discussed in this paper with consideration of the size, weight, and power limitations imposed by the satellite. An analysis was performed to study the torque errors associated with commercially available (COTS) gimbal and flywheel motors selected to meet the satellite imposed limitations as well as the mission requirements. A hybrid steering logic, which uses gyroscopic torque for rapid retargeting and direct torque of flywheel motors for precision pointing, was introduced and was shown through simulations to be a practical solution for rapid retargeting and precision pointing of small satellites using COTS components.

Future work involves prototyping and experimental testing of this system. Additionally, momentum management strategies will be developed to minimize flywheel speed drifts that may occur after multiple maneuvers.

References

1. W. J. Blackwell et al, "Nanosatellites For Earth Environmental Monitoring: The MicroMAS Project," In the proceedings from the 26th annual AIAA/USU conference on small satellites, Utah, 2012
2. Lars K et al, "GomX-1: A Nano Satellite Mission to Demonstrate Improved Situational Awareness for Air Traffic Control," In the proceedings from the 26th annual AIAA/USU conference on small satellites, Utah, 2012
3. Andrew Cawthorne et al, "Very High Resolution Imaging Using Small Satellites," In the proceedings from the 6th Responsive Space Conference, Los Angeles, CA, April 28–May 1, 2008
4. David B. Marks and Richard A. Fink, "DC Motor Selection for Space Mechanisms," In the proceedings of the 36th Aerospace Mechanisms Symposium, Glenn Research Center, May 15-17, 2002
5. Kunal Patankar and Norman Fitz-Coy, "A Hybrid CMG-RW Attitude Control Strategy for Agile Small Satellites," In the proceedings of the AAS/AIAA Astrodynamics Specialist Conference, Hilton Head, South Carolina, August 11-15, 2013
6. C. Salane and X. Roser, "AOCS for Agile Scientific Spacecraft with Mini CMG's," In the proceedings of the 4th ESA International Conference on Spacecraft Guidance, Navigation and Control Systems, ESTEC, Noordwijk, The Netherlands, October 18-21, 1999
7. D. Jung and P. Tsiotras, "An Experimental Comparison of CMG Steering Control Laws, " In the proceedings from the AIAA Astrodynamics Specialist Conference, 2004.
8. M.D. Kuhns and A.A. Rodriguez, "A Preferred Trajectory Tracking Steering Law for Spacecraft with Redundant CMGs," In the proceedings from the American Control Conference, 1995., volume 5, 1995.
9. J.A. Paradiso, "Global steering of single gimballed control moment gyroscopes using a directed search," *Journal of Guidance, Control, and Dynamics*, 15(5):1236–1244, 1992.
10. S. Asghar, PL Palmer, and M. Roberts, "Exact steering law for pyramid-type four control moment gyro systems," In the proceedings from the AIAA/AAS Astrodynamics Specialist Conference and Exhibit, Keystone, CO, 2006.
11. S.R. Vadali, S.R. Walker, and H.S. Oh, "Preferred gimbal angles for single gimbal control moment gyros," *Journal of Guidance, Control, and Dynamics*, 13(6):1090–1095, 1990.
12. B. Wie, D. Bailey, and C. Heiberg, "Singularity Robust Steering Logic for Redundant Single-Gimbal Control Moment Gyros," *Journal of Guidance, Control, and Dynamics*, 24(5):865–872, 2001.

13. B. Wie, D. Bailey, and C. Heiberg, "Rapid Multitarget Acquisition and Pointing Control of Agile Spacecraft," *Journal of Guidance, Control, and Dynamics*, 25(1):96–104, 2002.

14. K.A. Ford and C.D. Hall, "Singular Direction Avoidance Steering for Control-Moment Gyros," *Journal of Guidance, Control, and Dynamics* 23(4):648–656, 2000.

15. H. Schaub and J. Junkins, "Singularity Avoidance Using Null Motion and Variable-Speed Control Moment Gyros," *Journal of Guidance, Control, and Dynamics*, 23(1):11–16, 2002

16. B. Wie, H. Weiss, and A. Arapostathis, "Quaternion Feedback Regulator for Spacecraft Eigenaxis Rotations," *Journal of Guidance, Control, and Dynamics*, Vol. 12, No. 3, 1989, pp. 375–380.